# Modeling bending response of shape memory alloy wires/beams under superelastic conditions - A two species thermodynamic Preisach approach

## Ashwin Rao[*]

Department of Mechanical Engineering, Texas A&M University, College Station, TX 77843-3123, USA

## Abstract

In this paper, a model to capture the pure bending response of shape memory alloys (SMA) beams/wires under superelastic conditions is constructed by combining thermodynamics principles along with Preisach models. The model is formulated directly using experimentally measurable quantities "bending moment and curvature" rather than evaluating the same from stress resultants by integration as commonly followed in literature. Following Doraiswamy et al. Doraiswamy et al. (2011), the key idea here is in separating the thermoelastic and the dissipative part of the hysteretic response with a Gibbs potential based formulation and thermodynamic principles. The Preisach model is then employed in capturing the dissipative part of the response. Such an approach can simultaneously include both thermal and mechanical loading in the same framework and one can easily simulate complex temperature dependent superelastic responses. The model results are compared with experiments performed on SMA wires/beams at different temperatures as reported in the literature for NiTi and CuZnAl material systems.

Keywords : Shape memory alloy (SMA), bending, superelastic effect, Preisach model, design, bending moment, curvature

## 1  Introduction

Shape memory alloys (SMA) are a sub-group of adaptive materials whose functionalities arise from their underlying microstructural changes when subjected to changes in external non-mechanical stimuli like temperature, magnetic field etc. Wayman (1992). In thermally responsive SMAs, the reversible solid-solid phase transformations between a stable high temperature austenitic phase and low temperature martensitic phase are responsible for them

---

[*]Email : ashwintrr@gmail.com

to demonstrate interesting phenomenon like shape memory effect (SME) and superelasticity (SE) Lagoudas (2008). The use of such materials with combined sensing and actuation capabilities have enabled them to replace multicomponent systems to achieve the same desired functionality Ghosh et al. (2013). These unique characteristics of SME and SE have made SMAs find applications in sensing and control, vibration damping, biomedical, automotive and aerospace areas Song et al. (2006), Van Humbeeck (1999), Stoeckel (1990), Hartl and Lagoudas (2007).

SMAs are commonly used in the form of wires, springs, strips, sheets, tubings or bars under different loading conditions (tension, torsion or bending) for exploiting their unique characteristics in many practical applications Lagoudas (2008), Miyazaki and Otsuka (1989), NDC (2012). Due to SMA's excellent biocompatibility and corrosion resistance properties, the medical community in particular has found many applications for SMA in the form of self-expanding stents, spacers, guide-wires, atrial occlusion devices etc. Machado and Savi (2003), Morgan (2004), Bogue (2009). In many of these applications, SMAs are used under bending mode and thus efforts in understanding "force v/s deflection" responses has been of keen interest with the medical community. Experimental results for force v/s mid-span deflection for a 3-point bend test conducted on wires and slender beams have been reported widely by the biomedical community (see results in Brantley et al. (1978), Lopez et al. (1979), Drake et al. (1982), Goldberg et al. (1983), Asgharnia and Brantley (1986), Miura et al. (1986), Walia et al. (1988), Khier et al. (1991), Tonner and Waters (1994), Oltjen et al. (1997), Nakano et al. (1999), Wilkinson et al. (2002), Parvizi and Rock (2003), Garrec and Jordan (2004), Sakima et al. (2006), Bartzela et al. (2007)).

Based on these experimental evidences, researchers have suggested that due to SMAs superior spring-back properties, their ability to recover large deformations have potentially made them better alternatives compared to other material systems like stainless steel, $\beta$-Ti or Co-Cr for medical applications Drake et al. (1982), Miura et al. (1986), Kapila and Sachdeva (1989). Considering that most of the available experimental results are using 3-point bend tests, Berg Berg (1995), Rejzner et al.Rejzner et al. (2002) conducted experiments for a case of pure bending v/s curvature using custom designed experimental rigs. Wick et al. Wick et al. (1995) have also reported experimental results by comparing responses for 3-point bending, pure bending and tension loading cases (see figure 4 in Wick et al. (1995)).

In many of these applications, SMA components undergo repeated loading-unloading cycles and hence capturing their complex hysteretic responses is critical. Considering the importance of predicting the bending response with its associated hysteresis, some efforts towards modeling their complex response were undertaken.

Rejzner et al. Rejzner et al. (2002) used the model developed by Raniecki et al. (Raniecki et al. (2001)) to solve rate-type kinetic equations that takes into account tension-compression asymmetry along with a non-linear differential equation describing neutral plane motion for a symmetric cross-section. Marfia et al. Marfia et al. (2003) analysed a case of laminated SMA beams based on small-deformation Euler-Bernoulli theory. They explored a "mixture rule type approach" to determine martensite volume fractions and also established evolution equations for martensite and austentite phase production Marfia et al. (2003). They extend this approach

with Timoshenko theory to account for transverse shear and a layerwise approach which assumes constant shear deformation in beam cross-section. Axial force, bending moment and shear forces are derived as integrals of corresponding stress resultant expressions Marfia et al. (2003).

Atanacković and Achenbach Atanacković and Achenbach (1989), Eshghinejad and Elahinia Eshghinejad and Elahinia (2011) use an approach of dividing the phase transformation event into 3 different regions (elastic austentitc zone, a phase-transition region and an outer martensitic zone). Explicit relationships for bending moment are established upon integration of stress resultant expressions under loading and unloading events Atanacković and Achenbach (1989), Eshghinejad and Elahinia (2011).

Mirzaeifar et al. Mirzaeifar et al. (2012) in their recent work reduce the three dimensional constitutive equations developed by Boyd and Lagoudas Boyd and Lagoudas (1996), Qidwai and Lagoudas Qidwai and Lagoudas (2000) for a pure bending case. They consider two different transformation functions to account for tension-compression asymmetry and these constitutive relationships are reduced to appropriate forms to study SE effects Mirzaeifar et al. (2012). Closed form expressions for bending moment and curvature are analyzed analytically from these stress resultant expressions Mirzaeifar et al. (2012).

In all of the above mentioned approaches, expressions for bending moment are obtained by integrating explicit stress resultant equations established (in many cases reducing complex 3-D constitutive equations for a special tension–compression 1-D case). However, for a case of pure bending, as the wire/beam bends, the phase transformation front moves from the outer fiber towards the neutral axis (parallel to neutral axis) Rajagopal and Srinivasa (2005). As pointed out by Rao and Srinivasa Rao and Srinivasa (2013), the variation of the extent of transformation across the cross-section is not smooth and cannot be determined by easily integrating certain state variables in constitutive relations across the specimen cross sections Rao and Srinivasa (2013). They can be possibly determined only if the prior deformation history is known. Further, due to lack of full three-dimensional experimental data and tension-compression asymmetry, the approach of deriving moment–curvature relationships from stress resultants gets quite complicated. In addition, parameter identification in reduced 3-D models gets cumbersome due to lack of 3-D experimental data which forces approximations like the use of von-Mises equivalent stress approach for a 1-D reduction Rao and Srinivasa (2013). Given the complex thermomechanical nature of SMA responses, it is hard to justify the use of such von-Mises stress equivalent approaches as they have not performed well with even classical material systems Rao and Srinivasa (2013), Doaré et al. (2011).

Auricchio and Sacco Auricchio and Sacco (2001) developed a thermomechanical model to capture tension-bending superelastic response under small deformation theory assumptions that plane sections remain plane in both unreformed and deformed configurations Auricchio and Sacco (2001). However, axial forces and moments again are obtained from stress resultants by integration.

Purohit and Bhattacharya Purohit and Bhattacharya (2002) developed a strain energy relation that is a function of axial stretch, the average shear, and the curvature with the assumption the the beam is purely elastic Purohit and Bhattacharya (2002). They further

assume that the phase transformation front moves perpendicular and not parallel to the neutral axis Purohit and Bhattacharya (2002). This is contrary to the physical intuition of the way the transformation front moves across the cross-section (i.e parallel to neutral axis). This point has been discussed in detail by Rajagopal and Srinivasa Rajagopal and Srinivasa (2005) in their work where they develop finite deformation model for SMA beams. Rajagopal and Srinivasa Rajagopal and Srinivasa (2005) in their work assume a form for Helmholtz potential/unit mass with the assumption that the elastic constants of martensite and austenite are the same and do not vary with temperature. However, experimental evidences (3-point and pure bending experimental results) have illustrated that the superelastic responses are sensitive to temperature fluctuations and thus resulting in force variations for the same amount of deflection/curvature (see experimental results in Tonner and Waters (1994), Shaw and Kyriakides (1995), Parvizi and Rock (2003), Sakima et al. (2006)).

In order to overcome complexities of tension-compression asymmetry and temperature dependent SMA responses, a "simple mechanics of materials model for smart materials" based on experimentally measurable quantities "bending moment and curvature" is constructed by combining thermodynamics principles with Preisach models. Following the approach of Doraiswamy et al., Doraiswamy et al. (2011) the thermoelastic and the dissipative part of the hysteretic response are separated with a Gibbs potential based formulation and thermodynamic principles. The Preisach model is then employed in capturing the dissipative part of the response. Given the thermomechanical hysteretic nature of SMA response, pure elasticity theories considering mechanical loading alone are insufficient to capture such complex responses Rajagopal and Srinivasa (2005). The advancement from the classical beam theory is the inclusion of both thermal and mechanical loading in the same framework that can capture complex thermomechanical responses (refer fig 10 in Doraiswamy et al. (2011) for illustrations). Further, it is also capable of easily simulating both load and displacement controlled experiments with no further modifications to either the Gibbs potential or the actual model formulation. With minimum computations, one can capture stress and temperature driven phase changes when compared to complications involved with an equivalent 3-D model reduction to a special tension–compression case and further estimating bending moment from them. In addition, a model that is capable of accurately predicting bending moment v/s curvature response directly could facilitate designers greatly especially in designing SMA devices under superelastic conditions for many engineering applications.

## 2   Organization of this Paper

The remaining sections of the paper are organized as follows : In section 3, a Gibbs potential based model is developed to simulate superelastic response of SMA wires/beams in order to obtain "thermodynamic driving force and the volume fraction of martensite", by separating the thermoelastic and the dissipative part of the hysteretic response using thermodynamics principles. Further in section 4, details on employing a Preisach model to handle the dissipative part of the superelastic response is discussed. In section 5 , parameter identi-

fication for a given superelastic response is detailed. In section 6 , the simulation procedure is detailed with some highlights on salient features of the developed model. Next in section 7, the model predictions are compared against pure bending experimental results on SMA wires/beams obtained from Rejzner et al. (2002). Finally, in section 8, the highlights of this work are summarized.

# 3   Model Development

Consider a wire/beam subjected to pure bending with an applied bending moment "M" and its corresponding curvature denoted by "$\kappa$". Both bending moment "M" and curvature ($\kappa$) are experimentally determined.

## 3.1   The Gibbs Potential

A form for Gibbs potential per unit volume (inspired from Doraiswamy et al. (2011), Rajagopal and Srinivasa (1999)) is assumed and it is composed of the following terms (refer equation 3.1) :

1. a linear combination of the strain energy for the two phases,
2. an interaction term between the two phases,
3. a term related to the heat capacity difference between the two phases and
4. a term relating to the heat capacity of the austenite.

Specifically the Gibbs potential per unit reference volume is assumed to be of the form,

$$\mathcal{G} = -\overbrace{\left( \frac{\alpha M^2}{2E_m I} + \frac{(1-\alpha)M^2}{2E_a I} \right)}^{1} + \overbrace{B\alpha(\alpha - 1)}^{2} + \overbrace{(1-\alpha)(a+b\theta)}^{3} - \overbrace{C\theta(1 - \ln\theta)}^{4} \qquad (3.1)$$

where,
   - $\alpha$ is the martensite volume fraction during phase transformation,
   - M is the applied bending moment,
   - $E_a$ and $E_m$ are the austenitic and martensitic moduli,
   - $I = \frac{\pi d^4}{64}$ is the moment of inertia
   - $B, a$ and $b$ are constants,
   - $\theta$ is the temperature and
   - $C$ is the specific heat

The constant "B" represents the interaction energy between the austenite and martensite phases while "b" is the entropy difference between the austenite and martensite phases respectively (see equation 3.3 below). Constant "a" is the internal energy difference between the austenite and martensite phases at 0K (see equation 3.5 below). The method to identify the above parameters would be described later in section 5.

## 3.2   Establishing Driving Force

From classical thermodynamics, the entropy is given by,

$$\eta = -\frac{\partial \mathcal{G}}{\partial \theta} = -C \ln \theta - (1 - \alpha)b \tag{3.2}$$

Using above,

$$\left.\begin{array}{l} \eta|_{(\alpha=1)} = -C \ln \theta \\ \eta|_{(\alpha=0)} = -C \ln \theta - b \end{array}\right\} \Longrightarrow b = \Delta\eta = \eta|_{(\alpha=1)} - \eta|_{(\alpha=0)} \tag{3.3}$$

thus, $b$ is the entropy difference between the austenite and martensite states. The internal energy, $\exists$, is given by,

$$\exists = \mathcal{G} - \theta\frac{\partial \mathcal{G}}{\partial \theta} = -\left(\frac{\alpha M^2}{2E_m I} + \frac{(1-\alpha)M^2}{2E_a I}\right) + B\alpha(\alpha - 1) + (1 - \alpha)a - C\theta \tag{3.4}$$

Using above,

$$\left.\begin{array}{l} \exists_a = \exists|_{(\alpha=0, M=0, \theta=0)} = a \\ \exists_m = \exists|_{(\alpha=1, M=0, \theta=0)} = 0 \end{array}\right\} \Longrightarrow a = \exists_a - \exists_m \tag{3.5}$$

From the above, the parameter $a$ is the internal energy difference between the two phases at 0 K.

From the Gibbs potential, the elastic part of the total curvature is given by,

$$\kappa_e = -\frac{\partial \mathcal{G}}{\partial M} = \frac{\alpha M}{E_m I} + \frac{(1-\alpha)M}{E_a I} \tag{3.6}$$

Also, the Helmholtz potential $\psi$, is related to Gibbs potential $\mathcal{G}$, by,

$$\psi = G - M\frac{\partial \mathcal{G}}{\partial M} \tag{3.7}$$

The difference between the rate of external working ($M\dot{\kappa}$) and the rate of change of the Helmholtz potential keeping the temperature fixed ($\dot{\psi}|_\theta$), must be equal to the macroscopic inelastic power ($P_{inel}$).
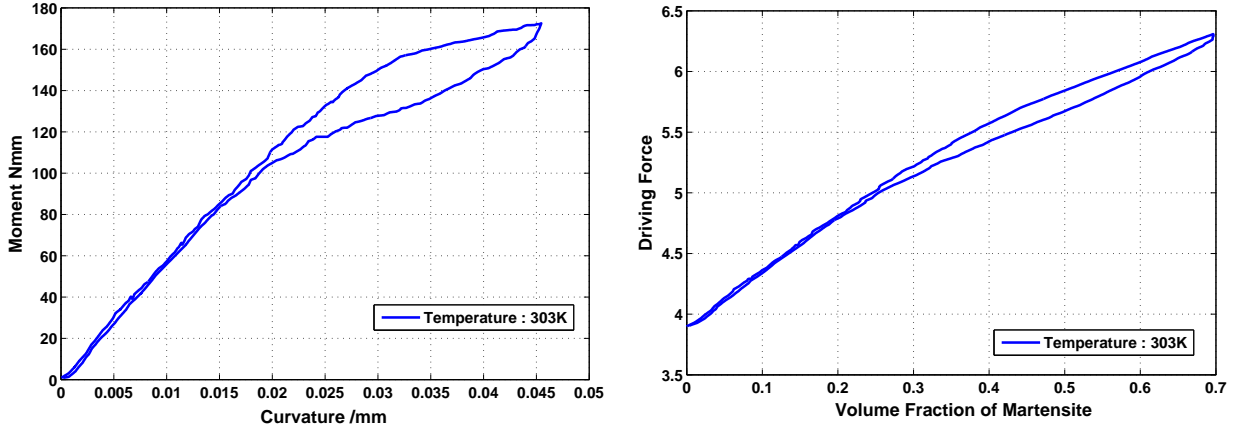
In other words,

$$P_{inel} = M\dot{\kappa} - \dot{\psi}|_\theta \tag{3.8}$$

Using equations 3.6, 3.7 in 3.8 and upon further simplification,

$$M(\dot{\kappa} - \dot{\kappa}_e) - \frac{\partial \mathcal{G}}{\partial \alpha}\dot{\alpha} = P_{inel} \tag{3.9}$$

From equation 3.9, it is observed that there are two contributions to the inelastic power, one from the shape change that occurs due to phase transition ($M(\dot{\kappa} - \dot{\kappa}_e)$) and the other from

(a) Bending moment v/s curvature plot at 303K Rejzner et al. (2002).

(b) Driving force – volume fraction plot

FIGURE 1 – Experimental bending moment v/s curvature data for NiTi wire is reduced to driving force–volume fraction plot using thermodynamic principles by using equations 3.15 and 3.14. (experimental data obtained from Rejzner et al. (2002).)

the energy difference between the two phases $\left(-\frac{\partial G}{\partial \alpha}\dot{\alpha}\right)$. The maximum transformational strain ($\kappa_{max}$ in this case)can assumed to be of the order of 6%.

$$\dot{\kappa} - \dot{\kappa}_e = \kappa_{max}\dot{\alpha} \Rightarrow \kappa - \kappa_e = \kappa_{max}\alpha \tag{3.10}$$

In the above equation note that, when $\alpha = 1$, $\kappa - \kappa_e = \kappa_{max}$ and when $\alpha = 0$, $\kappa - \kappa_e = 0$. Now substituting equation 3.10 into 3.9 we get.

$$\left(M\kappa_{max} - \frac{\partial \boldsymbol{G}}{\partial \alpha}\right)\dot{\alpha} = P_{inel} \tag{3.11}$$

It is now possible to identify the driving force for the phase transformation in the superelastic response of the SMA wires/beams :

$$\mathcal{F} = M\kappa_{max} - \frac{\partial \boldsymbol{G}}{\partial \alpha} \implies \mathcal{F}\dot{\alpha} = P_{inel} \tag{3.12}$$

$P_{inel}$ is the macroscopic inelastic power. The rate of dissipation, $\xi$, is the net macroscopic inelastic work in a closed cycle of state. In order to satisfy second law of thermodynamics, this quantity must be non-negative i.e,

$$\xi = \oint P_{inel}\,\mathrm{d}t \geq 0 \tag{3.13}$$

## 3.3   Driving Force & Volume Fraction Estimation using Experimental Data

Using equations 3.1 and 3.12, the driving force expression [1] can be established (given by equation 3.14 below) :

$$\mathcal{F} = M\kappa_{max} + M^2 \left( \frac{1}{2E_m I} - \frac{1}{2E_a I} \right) - B(2\alpha - 1) + b\theta + a \qquad (3.14)$$
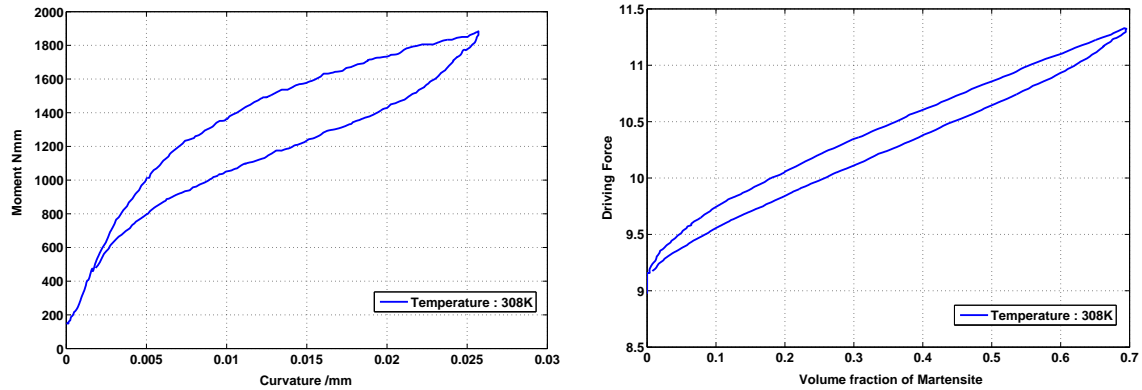
From equation 3.14, it is evident that driving force is a function of bending moment (M), curvature ($\kappa$) martensitic volume fraction ($\alpha$), and temperature ($\theta$). The variables bending moment, curvature and temperature are nondimensionalised prior to proceeding with further derivations. The nondimensionalised variables are : $M^* = M/M_{max}$, $\kappa^* = \kappa/\kappa_{max}$, $\theta^* = \theta/\theta_{max}$. Henceforth, for better readability, the $*$'s will be omitted from the nondimensionalised variables.

The martensitic volume fraction evolution ($\alpha$) given by equation 3.15 can be obtained using expressions 3.6 and 3.10.

$$\alpha = \frac{\kappa - \dfrac{M}{E_a I}}{\dfrac{M}{E_m I} - \dfrac{M}{E_a I} + 1} \qquad (3.15)$$

Experimental results for one particular temperature case are chosen as reference for simulation and establishment of driving force and volume fraction relationships. This can be achieved using expressions 3.14 and 3.15, where each experimental data point from experimental bending moment v/s curvature plot can be reduced to corresponding driving-force – volume fraction plot as shown in figures 1 and 2 i.e ($M, \kappa$) to ($\mathcal{F}, \alpha$). It must be highlighted that expressions 3.14 and 3.15 were a result of employing a thermodynamical framework typically used in modeling phase transforming materials. Now unlike a conventional "plasticity-like" approach where evolution equations for $\dot{\alpha}$ are established (see Boyd and Lagoudas (1996), Qidwai and Lagoudas (2000), Mirzaeifar et al. (2012)), a discrete Preisach model is employed in this case to capture changes in $\alpha$. The phase transformations in SMA can be perceived as switching events between two phases (austenite and martensite) and the use of Preisach models is quite appropriate here as these were developed to capture hysteresis effects due to "domain switching in magnetism" Rao and Srinivasa (2013). Further, such an approach solely focuses on the hysteretic dissipative part of the response and not on the entire response. Following Doraiswamy et al. Doraiswamy et al. (2011), the $\mathcal{F}-\alpha$ relationships can be modeled using the Preisach models.

---

1. Due to material heterogeneity and the assumption of phase transformation front being parallel to neutral axis, one can assume moment of inertia $I_m$ and $I_a$ for the two phases martensite and austenite respectively in the model formulation for general cases. However, due to paucity of experimental data on pure bending of SMA components (especially fully transformed cases), it hard to actually determine the individual values of $I_m$ and $I_a$ for model calibration. For simplicity, a common moment of inertia "I" estimated from the initial referential configuration is employed for both the phases. If more experimental data is made available, then one can consider $I_m$ and $I_a$ in the model formulation and relate them to the volume fraction of martensite $\alpha$ especially under fully transformed cases.

(a) Bending moment v/s curvature plot at 308K Rejzner et al. (2002).

(b) Driving force – volume fraction plot

FIGURE 2 – Experimental bending moment v/s curvature data for CuZnAl beam is reduced to driving force–volume fraction plot using thermodynamic principles by using equations 3.15 and 3.14. (experimental data obtained from Rejzner et al. (2002).)

# 4  Preisach Model Development

The Preisach model was first introduced by F. Preisach in 1935 to study hysteresis in magnetic materials. Mayergoyz Mayergoyz (2003) in his book "mathematical models of hysteresis" discusses the notion of substituting a smooth hysteresis curve with a series of steps and each step is referred to as a "hysteron" and characterized by three characteristic parameters namely the "On" condition, "Off" condition and "height of the step" Mayergoyz (1986). The traditional Preisach models assembles series of basic hysteretic elements or hysterons to simulate hysteresis either stress – strain Ortín (1992) or temperature – strain Ktena et al. (2001), Bo and Lagoudas (1999) relationships directly.

Following Doraiswamy et al. Doraiswamy et al. (2011), in this approach, each hysteron (see figure 3) behaves like a non-ideal switch that switches on when the load increases beyond $\mathcal{F}_{forward}$, giving an "output", $\Delta\alpha$, and switches off at $\mathcal{F}_{backward}$. With the establishment of the driving force and extent of transformation expressions (equations 3.14 and 3.15 respectively), the thresholds for the hysteron are $\mathcal{F}_{forward}$ and $\mathcal{F}_{backward}$ and the output being volume fraction. With the use of large number of hysterons in series that turn on and off at different driving force values, contribution of each hysteron to volume fractions can be obtained.

## 4.1  Algorithm for obtaining Preisach parameters

The algorithm employed by Doraiswamy et al. Doraiswamy et al. (2011) for obtaining Preisach parameters is briefly summarized in appendix A for the sake of completeness. The algorithm details the process by which the contribution of each hysteron is accumulated to get the total volume fraction of martensite for a given driving force.
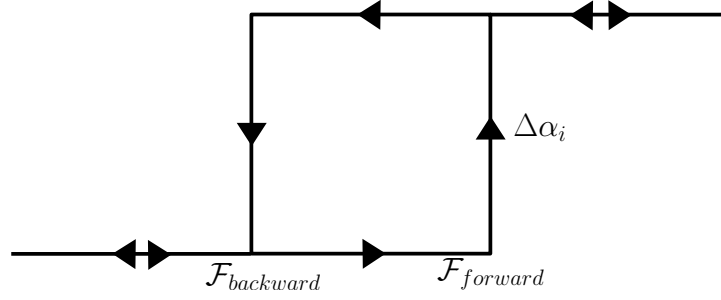
<span class="smallcaps">Figure</span> 3 – Basic hysteretic element or hysteron used in the Preisach Model. Directions of allowed transformations are represented by the arrows on the hysteron Doraiswamy et al. (2011).

## 4.2   Preisach Triangle

Following Doraiswamy et al. Doraiswamy et al. (2011), the Preisach triangle (see chapter 1 Mayergoyz (2003)) is a geometric interpretation of arranging hysterons in a systematic way allowing switch on and switch off of these elements. The hysterons are assigned $\mathcal{F}_{forward}$ and $\mathcal{F}_{backward}$ in a way such that the hysterons on any particular row have the same $\mathcal{F}_{forward}$ and the hysterons on any column have the same $\mathcal{F}_{backward}$ in the triangle. Further, the hysterons with the lowest $F_{forward}$ are positioned at the bottom row of the triangle, and the forward threshold value increases up along the rows. Similarly, the hysterons with the lowest $F_{backward}$ are positioned at the left end of the triangle, and the backward threshold values increase from left to right.

Once the $\mathcal{F}_{forward}$ and $\mathcal{F}_{backward}$ values are assigned, the corresponding "output", $\Delta\alpha$ for each hysteron are computed. Thus by assigning hysterons at specific positions on a Preisach triangle, the three parameters $\mathcal{F}_{forward}$, $\mathcal{F}_{backward}$ and $\Delta\alpha$ are automatically estimated. The number of hysterons in a triangle of side $n$ is $\frac{n(n+1)}{2}$.

In order to evaluate $\Delta\alpha$ for each hysteron, a system of equations are setup where each equation corresponds to the sum of the outputs of all those hysterons that are switched on. These are now equated to the volume fraction, $\alpha$ from the data (from figures 1(b) or 2(b)) corresponding to the driving force level. Since there are $\frac{n(n+1)}{2}$ hysterons, and only $k\left(<\frac{n(n+1)}{2}\right)$ data points (depending on the experimental data), the least squares fit with the non-negativity constraint for the outputs of the hysterons is computed using **"lsqnonneg"** package from MATLAB®. An example of assigning three parameters in a Preisach triangle of side 9 is illustrated in appendix B for more clarity.

# 5   Parameter Identification

By combining thermodynamics principles and Preisach modeling techniques, the model parameters can be separated into sets of parameters arising from the thermodynamical framework and those from the Preisach models related to hysterons positioning. Section 4 discussed the details of obtaining parameters $\mathcal{F}_{forward}$, $\mathcal{F}_{backward}$ and $\Delta\alpha$ pertaining to Preisach triangle as

represented in figure 3 by automatically assigning the hysterons at specific positions on the triangle.

The method of obtaining parameters arising from the assumed form of Gibbs potential (refer equation 3.1)from thermodynamical framework will be discussed below. The parameters under consideration $E_a$, $E_m$, $B$, $a$ and $b$ and their corresponding values used for simulation and model predictions are reported in table 1. The parameters are determined keeping the experimental data on pure bending of NiTi wire from Rejzner et al. Rejzner et al. (2002) as reference.

- "$E_a$" and "$E_m$" being the austenitic and martensitic elastic moduli can be estimated directly form the tension experimental data by finding the initial slopes of the superelastic response.
- "$B$" is the coefficient of the interaction energy term related to the area of hysteresis (as shown in Rajagopal and Srinivasa (1999)). Therefore parameter "$B$" is proportional to the area of hysteresis under bending moment v/s curvature plot. A value for "$B$" is chosen in order to obtain a good fit between the model and the experimental hysteresis.
- The computation of entropy difference "$b$" can justified by the comparing responses at two different temperatures as shown below. If $\mathcal{F}_1$ is the driving force at torque $M_1$ and temperature $\theta_1$ and $\mathcal{F}_2$ is the corresponding driving force at torque $M_2$ and $\theta_2$ respectively.

$$\mathcal{F}_1 = \frac{M_1^2}{2}\left(\frac{1}{E_m I} - \frac{1}{E_a I}\right) + a + b\theta_1 - B(2\alpha - 1) + M_1\kappa_{max} \tag{5.1}$$

$$\mathcal{F}_2 = \frac{M_2^2}{2}\left(\frac{1}{E_m I} - \frac{1}{E_a I}\right) + a + b\theta_2 - B(2\alpha - 1) + M_2\kappa_{max} \tag{5.2}$$

$$\mathcal{F}_1 - \mathcal{F}_2 = \frac{M_1^2 - M_2^2}{2}\left(\frac{1}{E_m I} - \frac{1}{E_a I}\right) + b(\theta_1 - \theta_2) + (M_1 - M_2)\kappa_{max} \tag{5.3}$$

The driving force analogous to chemical potential (see Callen (1985)) does not change with temperature and therefore $\mathcal{F}_1$ - $\mathcal{F}_2$=0. Using this relation and further neglecting the terms arising due to modulus differences, we get,

$$b = -\frac{M_1 - M_2}{\theta_1 - \theta_2}\kappa_{max}, \tag{5.4}$$

It can be seen that the value of "$b$" (from table 1) matches with the values available in the literature for SMA (see Bo et al. (1999)).

- The parameter "$a$" serves as a datum for the driving force and is computed by setting the driving force to be zero at the stress-free austenite phase i.e.,

$$\mathcal{F}|_{\alpha=0,M=0} = a + b\theta + B \tag{5.5}$$

$$a = -b\theta - B \tag{5.6}$$

TABLE 1 − Values of thermodynamical parameters employed for model verification for pure bending experimental data of NiTi wire Rejzner et al. (2002)

| Parameters | Corresponding Values |
|:---:|:---:|
| $E_a$ | 45 GPa |
| $E_m$ | 35 GPa |
| $B$ | -1.33 Nmm |
| $a$ | 44.3 Nmm |
| $b$ | -0.133 Nmm/K |
| $\theta_1$ | 323 K |
| $\theta_2$ | 303 K |

# 6    Bending Moment vs Curvature - Simulations & Model Predictions

The algorithm described in appendix A is used to estimate the volume fraction $\alpha$ for a given driving force $\mathcal{F}$. The process of finding the original bending moment vs curvature using the above algorithm is detailed below for specific experimental protocols (load and displacement tests). Further, it must be highlighted that both load and displacement controlled experiments (sections 6.1 and 6.2 below) can be captured with no further modifications to either the Gibbs potential or the actual model formulation discussed thus far. For prediction of responses considered here, a total of 11325 hysterons were used (i.e an equivalent of a Preisach triangle with a side of 150). The model predictions can be tailored by controlling the size of Preisach triangle for a smooth or a jagged response at the cost of computational time

## 6.1    Load (Moment) Controlled Protocol

If at time $t_i$, M(i), $\kappa(i)$ and $\theta(i)$ are assumed to be known then by using equation 3.15, $\alpha(i)$ can be evaluated. In order to compute these variables at time $t_{i+1}$, it is assumed that M(i+1) is known. $\mathcal{F}(i+1)$ can now be computed from equation 3.14 for a known $\alpha(i)$. Once $\mathcal{F}(i+1)$ is evaluated, the Preisach model is used to predict $\alpha(i+1)$. With $\alpha(i+1)$ and M(i+1) now known, using equation 3.6 to find $\kappa_e(i+1)$ and hence $\kappa(i+1)$ from equation 3.10. Summarizing the above we need to evaluate the equations below

$$\alpha^{(n)} = \sum_{i=0}^{n} \alpha_i^{(n)} \tag{6.1a}$$

$$\mathcal{F}^{(n+1)} = M^{(n+1)} + \left(M^{(n+1)}\right)^2 \left(\frac{1}{2E_mI} - \frac{1}{2E_aI}\right) - B\left(2\alpha^{(n)} - 1\right) + b\theta + a \tag{6.1b}$$

$$\kappa^{(n+1)} = \frac{\alpha^{(n)}M^{n+1}}{E_mI} + \frac{\left(1 - \alpha^{(n)}\right)M^{n+1}}{E_aI} + \alpha^n \tag{6.1c}$$

## 6.2 Displacement (Curvature) Controlled Protocol

If at time $t_i$, M(i), $\kappa(i)$ and $\theta(i)$ are known then by using equation 3.15 $\alpha(i)$ can be evaluated. Here $\kappa(i+1)$ is known and M(i+1) needs to be computed. $\mathcal{F}(i+1)$ is computed using equation 3.14. Now the equation 3.15 is used to express M in terms of $\kappa$ and $\alpha$. The Preisach model is used again to find $\alpha(i+1)$ from $\mathcal{F}(i+1)$. Once $\alpha(i+1)$ and $\kappa(i+1)$ are evaluated, using equation 3.15, M(i+1) is evaluated. Summarizing the above we need to evaluate the equations below

$$\alpha^{(n)} = \sum_{i=0}^{n} \alpha_i^{(n)} \tag{6.2a}$$

$$M^{(n+1)} = \frac{\kappa^{(n+1)} - \alpha^{(n)}}{\alpha^{(n)}\left(\frac{1}{E_m I} - \frac{1}{E_a I}\right) + \frac{1}{E_a I}} \tag{6.2b}$$

$$\mathcal{F}^{(n+1)} = M^{(n+1)} + \left(M^{(n+1)}\right)^2 \left(\frac{1}{2E_m I} - \frac{1}{2E_a I}\right) - B\left(2\alpha^{(n)} - 1\right) + b\theta + a \tag{6.2c}$$

## 6.3 Prediction at different temperatures

The volume fraction $\alpha$ and driving force $\mathcal{F}$ are estimated from the original bending moment vs curvature experimental data for a given temperature say $\theta_1$. The prediction of responses at different temperatures say $\theta_2$ or $\theta_3$ can be achieved by just "changing the temperature term" during the reverse calculations of bending moment vs curvature data from the $\mathcal{F} - \alpha$ generated for temperature $\theta_1$. Thus the hysteron parameters have to be estimated only once and they do not have to be recomputed for predictions at different temperatures.

# 7 Results and Discussion

## 7.1 Simulations of NiTi SMA wire and CuZnAl SMA Beam response using complete Bending Moment v/s Curvature data

Figure 4 shows the model simulation predictions as compared with experimental results at 303K for NiTi wire. Figure 5 shows the model simulation results at 308K for CuZnAl beam as compared with the corresponding experimental results. The model shows a good fit with the experimental results and can estimate the hysteresis accurately for both NiTi and CuZnAl material system. The close match of simulation results shows the power of Preisach model since the Preisach parameters were chosen to fit the data. The jaggedness in the response is due to employment of a discrete Preisach model in simulation. Experimental results for both cases were obtained from Rejzner et al. (2002).
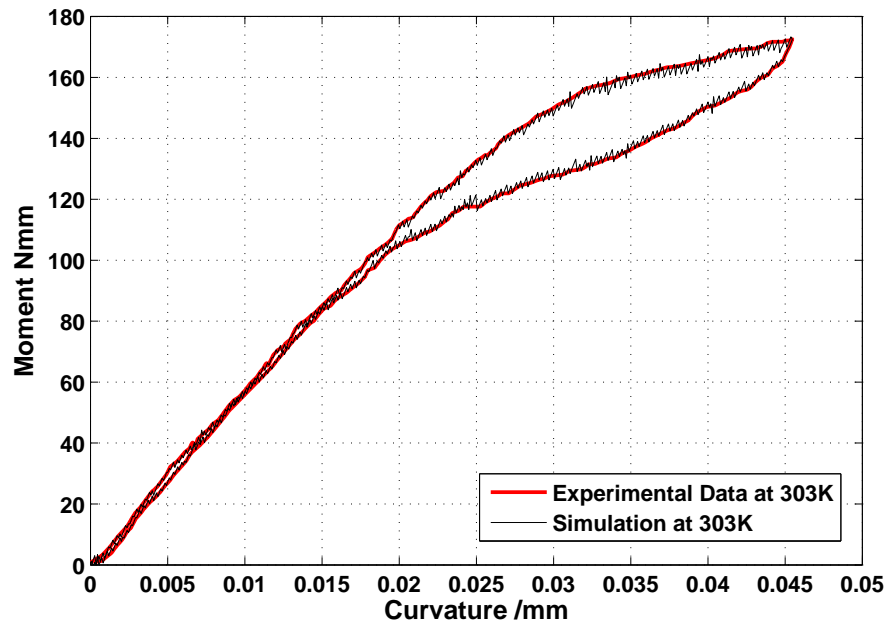
FIGURE 4 − Model prediction for the superelastic response of NiTi SMA wire at 303K. Model prediction and experimental results show a close match. The close match of simulation results shows the power of Preisach model since the Preisach parameters were chosen to fit the data. Experimental results at 303K were obtained from Rejzner et al. (2002).
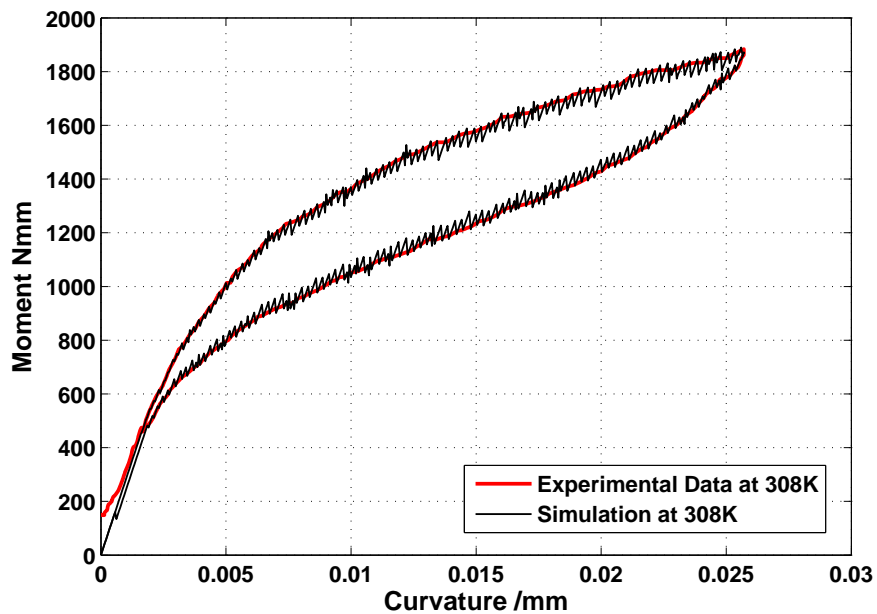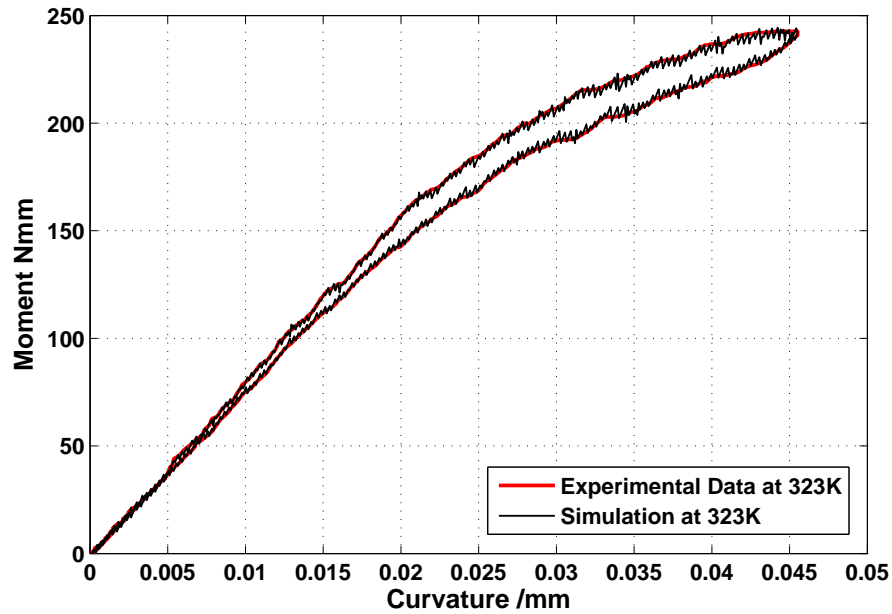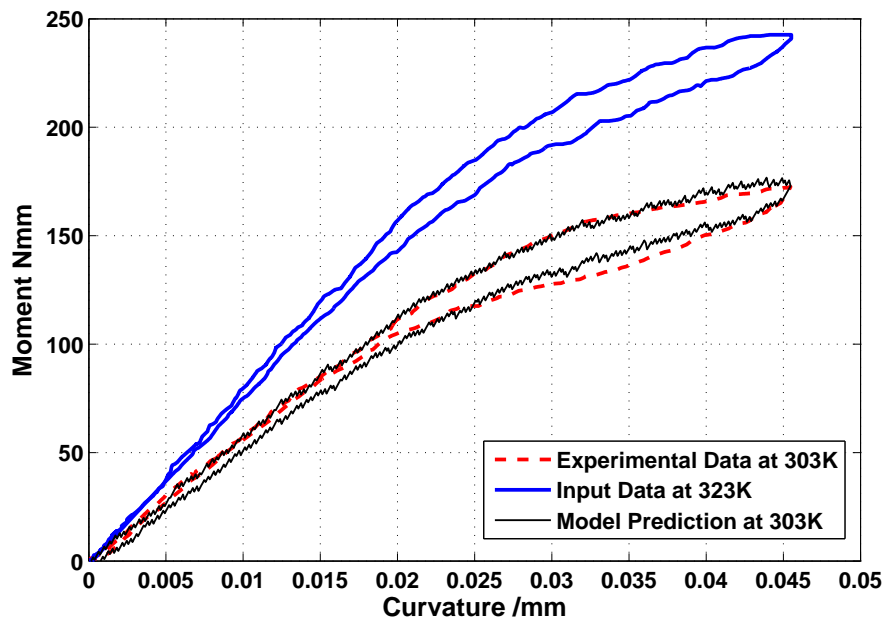


FIGURE 5 − Model prediction for the superelastic response of Cu-Zn-Al SMA beam tested at 308K showing a good match. The jaggedness in the response is due to employment of a discrete Preisach model in simulation. Experimental results at 308K were obtained from Rejzner et al. (2002).
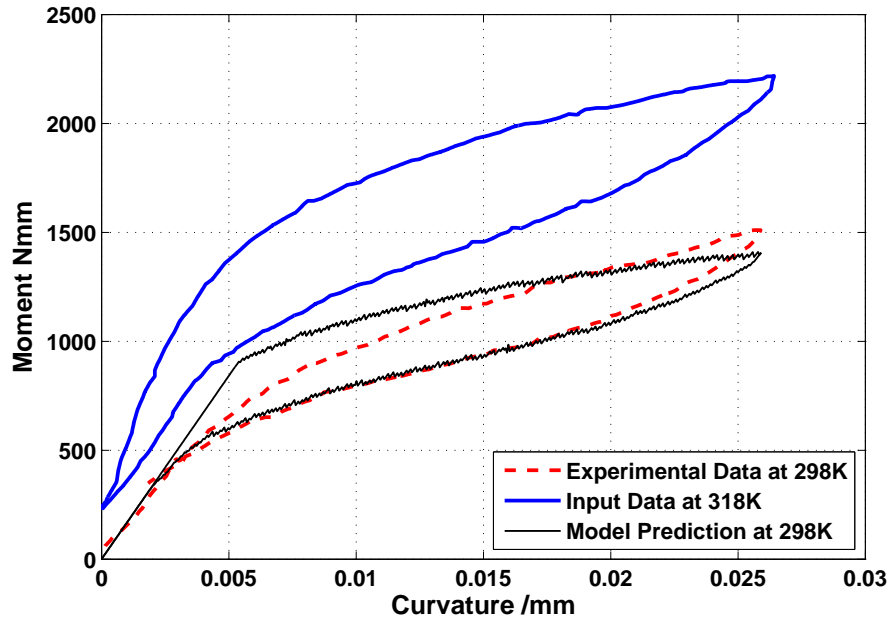
(a) Model prediction for 323K compared with the corresponding experimental data at 323K
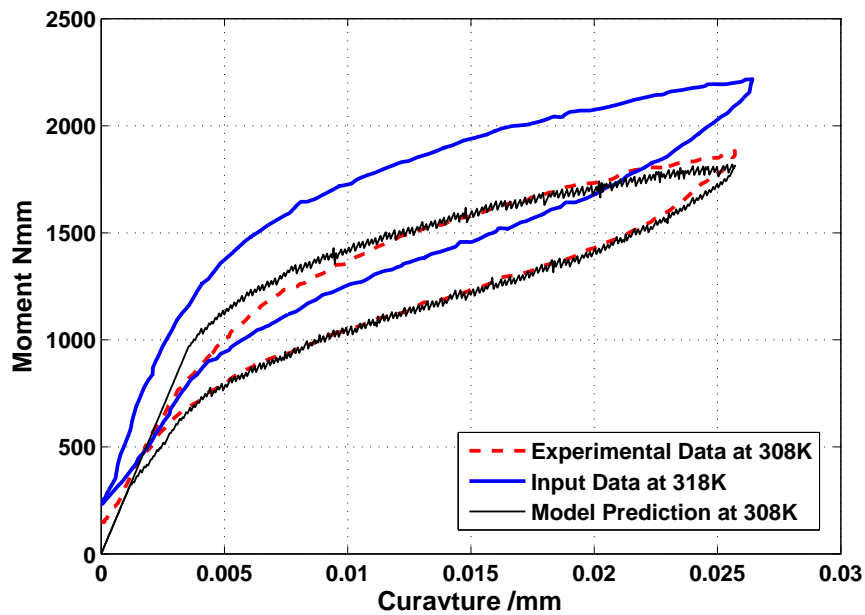


(b) Model prediction for 303K comapred with corresponding experimental results using the data at 323K as input. The average error for this case between the model predictions and experimental results was ∼ 8%

FIGURE 6 − Prediction for responses at temperatures 323 and 303K for a NiTi Specimen using the hysterons generated from 323K. It must be noted that the extent of transformation at 323K is different when compared to that in case of 303K. The results for both temperatures were obtained from Rejzner et al. (2002) (details in section 7.2)

(a) Model prediction for 298K using the input data at 318K



(b) Model prediction for 308K using the input data at 318K

FIGURE 7 – Prediction for responses for a CuZnAl specimen at temperatures 298 and 308K using the hysterons generated at 318K. It is observed from the reported experimental results at 318K and 308K that the specimen is subjected to a finite bending moment even at zero curvature (see figure 7 in Rejzner et al. (2002)). This affects the predictions as the observed elastic behaviour in CuZnAl case is much smaller when compared to NiTi case. This can be observed in the predictions of 298K results where the elastic part of the response is over-predicted. The average error for both cases between the model predictions and experimental results was ~ 16%. The results for both temperatures were obtained from Rejzner et al. (2002)

## 7.2 Simulation of NiTi SMA wire response at different temperatures

Figures 6(a) and 6(b) shows the model prediction at temperatures 323K and 303K using the hysterons generated with the 323K results as the data input. The hysteron parameters in this current estimation do not have to recomputed to predict the response at different temperatures. It is evident from the experimental results, that the higher the temperature above $A_f$, the lesser is the transformation from austentite to stress induced martensite (SIM) and thus lesser is hysteresis area when compared against the same maximum curvature $\kappa =$ 0.045 $mm^{-1}$ as reported by Rejzner et al. Rejzner et al. (2002). The NiTi wires undergo only a partial transformation from austenite to SIM at different temperatures above $A_f$ and thus the "extent of transformation" at 323K is different when compared to that of 303K result. The model predictions for different temperatures could match exactly if the superelastic responses at different temperatures are compared for the "same extent of transformation" for each temperature case. The model predictions at different temperatures would be over or under estimated based on the choice of temperature that is used to generate the hysterons for prediction. If one needs to predict the hysteresis exactly for a partially transformed case then one would have to recompute the hysterons for the each temperature case as described earlier in section 7.1.

## 7.3 Simulation of CuZnAl SMA beam response at different temperatures

Figures 7(a) and 7(b) shows the model prediction at temperatures 298K and 308K using the hysterons generated with the 318K results as the data input. Again, the hysteron parameters for this estimation do not have to recomputed to predict the responses at different temperatures. It is observed from the reported experimental results at 318K and 308K, that the specimen is subjected to a finite bending moment even at zero curvature (see figure 7 in Rejzner et al. (2002)). This affects the predictions as the observed elastic behaviour in CuZnAl case is much smaller when compared to NiTi case. This can be observed in 298K predictions, where the elastic part of the response is over-predicted. Further, the maximum applied curvature was in the range of 0.027 to 0.03 $mm^{-1}$ for different temperature trials reported by Rejzner et al. Rejzner et al. (2002). This suggests that the "extent of transformation" is different for each temperature case and hence resulting in over or under prediction of the hysteresis based on the trial (318K experimental results in this case) chosen to generate the hysterons for prediction of responses at other temperatures.

## 7.4 Average error estimation : Model prediction v/s Experimental results

It is evident that the model predictions do not exactly match the experimental results as discussed with results in sections 7.2 and 7.3. Since, hysterons generated from one experimental result are used as input data, an average error between the model prediction and the corresponding experimental results were estimated for each case under the given test conditions (see equation 7.1 below). The average errors were estimated using the trapezoidal

integration rule (trapz command in MATLAB®).

$$\text{Average error} = \sqrt{\frac{\int (\text{Model value} - \text{experimental value})^2 \, dx}{\left( \int \text{Experimental value} \right)^2 \, dx}} \tag{7.1}$$

The average error is an estimate for that specific case as the model predictions could be different depending on the hysterons calculated for predictions (i.e the choice of initial experimental data as input). The average error for each of model predictions discussed in this work are highlighted in figures 6(b) and 7.

# 8   Conclusions

In this paper, a model is constructed to capture the pure bending response of shape memory alloy beams/wires by combining thermodynamics principles along with Preisach models. The model is constructed based on experimentally measurable quantities bending moment and curvature, rather than solving for them from stress resultants upon integration as commonly followed in the literature. The key idea here was in separating the thermoelastic and the dissipative part of the hysteretic response with a two species Gibbs potential based formulation and further employing a discrete Preisach model for capturing the hysteretic part of the response. Such an approach can simultaneously include both thermal and mechanical loading in a single modeling framework with the capability of simulating both load and displacement controlled experiments. Further it allows for easy handling of temperature variations observed in superelastic responses of SMA. The model results are compared against experimental results reported in the literature on NiTi SMA wires and CuZnAl beams at different temperatures. An average error between the model predictions and corresponding experimental results were estimated for each case. The error estimation is specific for each comparison case based on the test conditions and the experimental trial initially chosen for model predictions or generation of hysterons. Prediction of bending moment v/s curvature response of SMA beams and wires directly could greatly facilitate designers in designing components for various engineering applications.

# 9   Acknowledgements

**Appendix**

# A    Preisach Algorithm

The algorithm employed by Doraiswamy et al. Doraiswamy et al. (2011) for obtaining Preisach parameters is briefly summarized below for the sake of completeness.
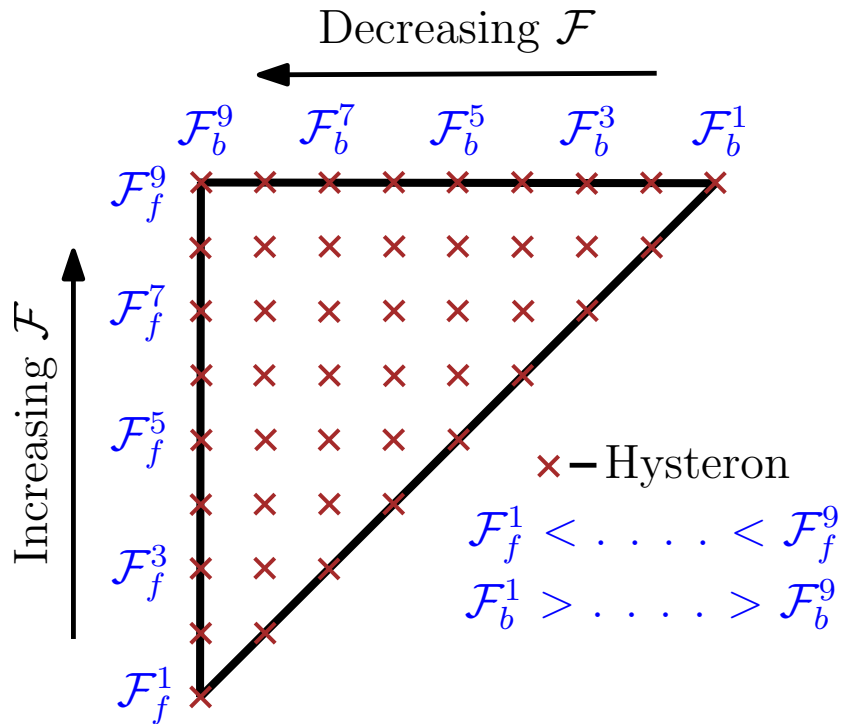


FIGURE 8 − Preisach Triangle : A systematic way for assigning switch on and switch off of the hysterons. The directions of loading (forward) and unloading (backward) sweeps are marked on the figure.

The state $S_i$ of the 'i'-th hysteron can take on one of two values : 0 or $\Delta \alpha^i$ where $\Delta \alpha^i$ is the volume fraction of martensite contributed by the 'i'-th hysteron. At any stage, the extent of transformation, i.e, the volume fraction of martensite evolved, is given by :

$$\alpha = \sum_{i=1}^{n} S_i \tag{A.1}$$

The state $S_i^{(n)}$ at time $t_n$ is known and hence the state at $t_{n+1}$ is given by :

$$\text{if } S_i^{(n)} = 0 \ \& \ \mathcal{F}^{(n+1)} > F_{forward}^i \tag{A.2}$$

$$\text{then } S_i^{(n+1)} = \Delta\alpha_i \tag{A.3}$$

$$\text{if } S_i^{(n)} = \Delta\alpha_i \ \& \ \mathcal{F}^{(n+1)} < F_{backward}^i \tag{A.4}$$

$$\text{then } S_i^{(n+1)} = 0 \tag{A.5}$$

$$\text{else } S_i^{(n+1)} = S_i^{(n)} \tag{A.6}$$

At the end of this time step, the $\alpha^{(n+1)}$ is then (as in A.1),

$$\alpha^{(n+1)} = \sum_{i=1}^{n} S_i^{(n+1)} \tag{A.7}$$

Thus, at the end of the time step $t_{n+1}$, $\alpha^{(n+1)}$ is known, given $\mathcal{F}^{(n+1)}$ and $S_i^{(n)}$ for all the hysterons. For each hysteron, inelastic power $\delta P_{inel}^i$ is given by,

$$\delta P_{inel}^i = \mathcal{F}\delta\alpha \tag{A.8}$$

$$= (\mathcal{F} - \mathcal{F}_{mean})\delta\alpha + \mathcal{F}_{mean}\delta\alpha \tag{A.9}$$

where $\delta\alpha$ is

$$\Delta\alpha_i \text{ if } \mathcal{F} > \mathcal{F}_{forward}^i \text{ or}$$
$$-\Delta\alpha_i \text{ if } \mathcal{F} < \mathcal{F}_{backward}^i.$$

Therefore, the first term in equation A.9 is always positive and the second term is positive or negative depending on $\delta\alpha$. The dissipation in a closed cycle of state (i.e sum of $\delta P_{inel}^i$ over all hysterons) will always be positive as the first term will be positive whereas the sum of second term will be zero. Using the above algorithm, the three parameters $\mathcal{F}_{forward}^i$, $\mathcal{F}_{backward}^i$ and $\Delta\alpha^i$ are computed for each hysteron and the driving forces ($\mathcal{F}_{forward}^i$, $\mathcal{F}_{backward}^i$) assigned in a systematic way as described in figure 8. This greatly simplifies the computation of $\Delta\alpha^i$ for each of the hysterons.

# B    Preisach Triangle : Example

Following Doraiswamy Doraiswamy (2010), a Preisach triangle of side 9 having 45 unknowns as shown in figure 9 is considered for illustration of automatically assigning the three parameters $\mathcal{F}_{forward}$, $\mathcal{F}_{backward}$ and $\Delta\alpha$. If the points are assumed as shown below :
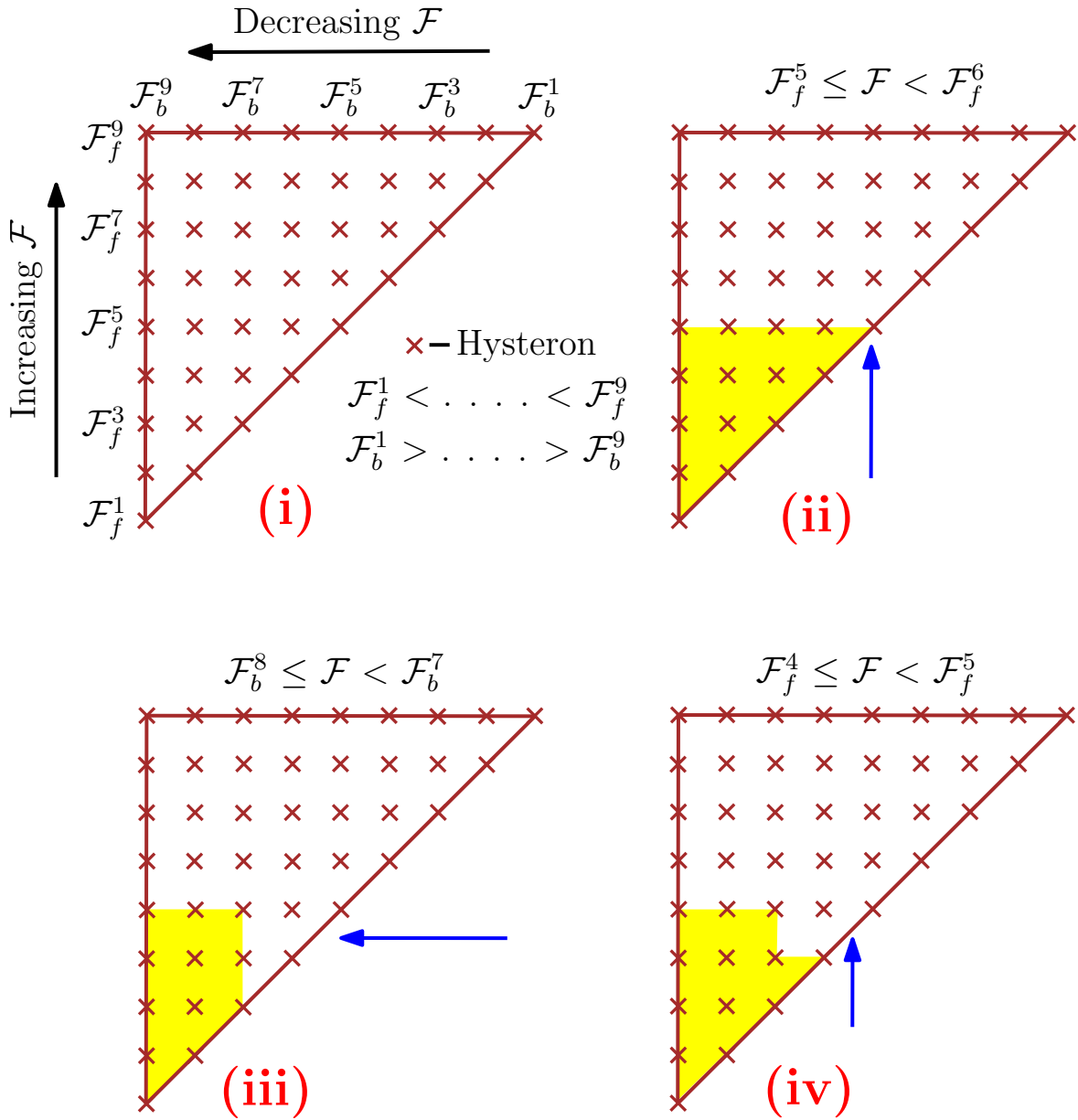
FIGURE 9 − (i) : Preisach triangle - A systematic way for assigning switch on and switch off of the hysterons. The directions of loading (forward) and unloading (backward) sweeps are marked on the figure. Sub figures (ii), (iii), (iv) shows an example for sequencing of states in the Preisach triangle. The colored section shows the hysterons that are switched on with the corresponding driving force enforcing the state at the top of the state.

$$
\mathcal{F} = \begin{bmatrix} 0 \\ \vdots \\ \mathcal{F}_1 \\ \vdots \\ \mathcal{F}_2 \\ \vdots \\ \mathcal{F}_3 \\ \vdots \end{bmatrix}_{n \times 1}
\qquad
\alpha = \begin{bmatrix} 0 \\ \vdots \\ \alpha_1 \\ \vdots \\ \alpha_2 \\ \vdots \\ \alpha_3 \\ \vdots \end{bmatrix}_{n \times 1}
$$

As shown in figure 9 (i), the first entry is assigned as 0 and none of the hysterons are switched on. If a state ($\mathcal{F}_f^5 \leq \mathcal{F} < \mathcal{F}_f^6$) shown in figure 9 (ii) is assumed and if $\mathcal{F}_1$ be the corresponding driving force, then $\alpha_1$ is the evolved volume fraction a that state. The hysterons contributing to $\alpha_1$ based on the highlighted area in figure 9 (ii) and the algorithm described earlier in appendix A.

$$
\Delta \alpha_1 = \Delta \alpha_{11} + \Delta \alpha_{21} + \Delta \alpha_{22} + \Delta \alpha_{31} + \Delta \alpha_{32} + \Delta \alpha_{33} + \Delta \alpha_{41} + \Delta \alpha_{42}
$$
$$
+ \Delta \alpha_{43} + \Delta \alpha_{44} + \Delta \alpha_{51} + \Delta \alpha_{52} + \Delta \alpha_{53} + \Delta \alpha_{54} + \Delta \alpha_{55}
\tag{B.1}
$$

where $\Delta \alpha_{ij}$ corresponds to the hysteron at the $i$-th row from bottom and $j$-th column from the left. Similarly one can write equations for $\alpha_2$ and $\alpha_3$ corresponding to cases depicted in figures 9 (iii) and 9 (iv) respectively. In order to evaluate $\Delta \alpha$ for each hysteron, a system of equations are setup, where each equation corresponds to sum of all outputs of those hysterons that are switched on. The entire system can be expressed as follows $Ax = B$.

$$
\underbrace{\begin{bmatrix} 0 & & \cdots & & 0 \\ & & \vdots & & \\ 1 & 1 & \cdots & 1 & 0 & \cdots & 0 \\ & & \vdots & & \\ 1 & 1 & & \cdots & & 1 & 1 \end{bmatrix}_{n \times 45}}_{\mathbf{A}}
\underbrace{\begin{bmatrix} \Delta \alpha_{11} \\ \vdots \\ \Delta \alpha_{55} \\ \vdots \\ \Delta \alpha_{99} \end{bmatrix}_{45 \times 1}}_{\mathbf{x}}
=
\underbrace{\begin{bmatrix} 0 \\ \vdots \\ \alpha_1 \\ \vdots \\ 1 \end{bmatrix}_{n \times 1}}_{\mathbf{B}}
$$

It is clear that there are $\frac{n(n+1)}{2}$ hysterons, and only $k \left( < \frac{n(n+1)}{2} \right)$ data points (depending on the experimental data) are available. In this example, the dimensions of A are $k \times 45$ and with $k < \frac{n(n+1)}{2}$, it is not possible to inverse the relationship as $x = A^{-1}b$. This problem is solved using least squares technique.

$$
\text{minimize } \| Ax - b \|
$$
$$
\text{subject to} \quad x_i > 0 \ \forall \ i = 1, \cdots, \frac{n(n+1)}{2}
\tag{B.2}
$$

The constrained least square problem is formulated as shown in equation B.2 with the non-negativity constraint for the outputs of the hysterons computed using **"lsqnonneg"** package from MATLAB®.

# **Références**

Asgharnia, M. and W. Brantley, 1986 : Comparison of bending and tension tests for orthodontic wires. *American Journal of Orthodontics*, **89 (3)**, 228–236.

Atanacković, T. and M. Achenbach, 1989 : Moment-curvature relations for a pseudoelastic beam. *Continuum Mechanics and Thermodynamics*, **1 (1)**, 73–80.

Auricchio, F. and E. Sacco, 2001 : Thermo-mechanical modelling of a superelastic shape-memory wire under cyclic stretching–bending loadings. *International Journal of Solids and Structures*, **38 (34)**, 6123–6145.

Bartzela, T., C. Senn, and A. Wichelhaus, 2007 : Load-deflection characteristics of superelastic nickel-titanium wires. *The Angle orthodontist*, **77 (6)**, 991–998.

Berg, B., 1995 : Bending of superelastic wires, part i : Experimental aspects. *Journal of applied mechanics*, **62**, 459.

Bo, Z. and D. Lagoudas, 1999 : Thermomechanical modeling of polycrystalline smas under cyclic loading, part iv : Modeling of minor hysteresis loops. *International Journal of Engineering Science*, **37 (9)**, 1205–1249.

Bo, Z., D. C. Lagoudas, and D. Miller, 1999 : Material characterization of sma actuators under nonproportional thermomechanical loading. *Journal of Engineering Materials and Technology*, **121 (1)**, 75–85.

Bogue, R., 2009 : Shape-memory materials : a review of technology and applications. *Assembly Automation*, **29 (3)**, 214–219.

Boyd, J. and D. Lagoudas, 1996 : A thermodynamical constitutive model for shape memory materials. part i. the monolithic shape memory alloy. *International Journal of Plasticity*, **12 (6)**, 805–842.

Brantley, W., W. Augat, C. Myers, and R. Winders, 1978 : Bending deformation studies of orthodontic wires. *Journal of Dental Research*, **57 (4)**, 609.

Callen, H., 1985 : Thermodynamics and an introduction to thermostatistics. *Thermodynamics and an Introduction to Thermostatistics, 2nd Edition, by Herbert B. Callen, pp. 512. ISBN 0-471-86256-8. Wiley-VCH, August 1985.*

Doaré, O., A. Sbarra, C. Touzé, M. Moussa, and Z. Moumni, 2011 : Experimental analysis of the quasi-static and dynamic torsional behaviour of shape memory alloys. *International Journal of Solids and Structures*.

Doraiswamy, S., 2010 : Discrete preisach model for the superelastic response of shape memory alloys. M.S. thesis, Texas A&M University.

Doraiswamy, S., A. Rao, and A. Srinivasa, 2011 : Combining thermodynamic principles with preisach models for superelastic shape memory alloy wires. *Smart Materials and Structures*, **20**, 085 032.

Drake, S., D. Wayne, J. Powers, and K. Asgar, 1982 : Mechanical properties of orthodontic wires in tension, bending, and torsion. *American Journal of Orthodontics*, **82 (3)**, 206–210.

Eshghinejad, A. and M. Elahinia, 2011 : Exact solution for bending of shape memory alloy superelastic beams. *ASME Conference Proceedings*, **2011 (54723)**, 345–352, doi : 10.1115/SMASIS2011-5151, URL `http://link.aip.org/link/abstract/ASMECP/v2011/i54723/p345/s1`.

Garrec, P. and L. Jordan, 2004 : Stiffness in bending of a superelastic ni-ti orthodontic wire as a function of cross-sectional dimension. *The Angle Orthodontist*, **74 (5)**, 691–696.

Ghosh, P., A. Rao, and A. R. Srinivasa, 2013 : Design of multi-state and smart-bias components using shape memory alloy and shape memory polymer composites. *Materials & Design*, **44**, 164–171.

Goldberg, A., J. Morton, and C. Burstone, 1983 : The flexure modulus of elasticity of orthodontic wires. *Journal of Dental Research*, **62 (7)**, 856–858.

Hartl, D. and D. Lagoudas, 2007 : Aerospace applications of shape memory alloys. *Proceedings of the Institution of Mechanical Engineers, Part G : Journal of Aerospace Engineering*, **221 (4)**, 535.

Kapila, S. and R. Sachdeva, 1989 : Mechanical properties and clinical applications of orthodontic wires. *American Journal of Orthodontics and Dentofacial Orthopedics*, **96 (2)**, 100–109.

Khier, S., W. Brantley, and R. Fournelle, 1991 : Bending properties of superelastic and nonsuperelastic nickel-titanium orthodontic wires. *American Journal of Orthodontics and Dentofacial Orthopedics*, **99 (4)**, 310–318.

Ktena, A., D. Fotiadis, P. Spanos, and C. Massalas, 2001 : A preisach model identification procedure and simulation of hysteresis in ferromagnets and shape-memory alloys. *Physica B : Condensed Matter*, **306 (1)**, 84–90.

Lagoudas, D., 2008 : *Shape memory alloys : modeling and engineering applications*. Springer Verlag.

Lopez, I., J. Goldberg, and C. Burstone, 1979 : Bending characteristics of nitinol wire. *American journal of orthodontics*, **75 (5)**, 569.

Machado, L. and M. Savi, 2003 : Medical applications of shape memory alloys. *Brazilian Journal of Medical and Biological Research*, **36 (6)**, 683–691.

Marfia, S., E. Sacco, and J. Reddy, 2003 : Superelastic and shape memory effects in laminated shape-memory-alloy beams. *AIAA journal*, **41 (1)**, 100–109.

Mayergoyz, I., 1986 : Mathematical models of hysteresis. *Magnetics, IEEE Transactions on*, **22 (5)**, 603–608.

Mayergoyz, I., 2003 : *Mathematical models of hysteresis and their applications*. Academic Press.

Mirzaeifar, R., R. DesRoches, A. Yavari, and K. Gall, 2012 : A closed-form solution for superelastic shape memory alloy beams subjected to bending. *Proceedings of SPIE*, Vol. 8342, 83421O.

Miura, F., M. Mogi, Y. Ohura, and H. Hamanaka, 1986 : The super-elastic property of the japanese niti alloy wire for use in orthodontics. *American Journal of Orthodontics and Dentofacial Orthopedics*, **90 (1)**, 1–10.

Miyazaki, S. and K. Otsuka, 1989 : Development of shape memory alloys. *ISIJ International*, **29 (5)**, 353–377.

Morgan, N., 2004 : Medical shape memory alloy applicationsthe market and its products. *Materials Science and Engineering : A*, **378 (1)**, 16–23.

Nakano, H., K. Satoh, R. Norris, T. Jin, T. Kamegai, F. Ishikawa, and H. Katsura, 1999 : Mechanical properties of several nickel-titanium alloy wires in three-point bending tests. *American journal of orthodontics and dentofacial orthopedics*, **115 (4)**, 390–395.

NDC, 2012 : Company website. `http://www.nitinol.com/`.

Oltjen, J., M. Duncanson Jr, J. Ghosh, R. Nanda, and G. Frans Currier, 1997 : Stiffness-deflection behavior of selected orthodontic wires. *The Angle Orthodontist*, **67 (3)**, 209–218.

Ortín, J., 1992 : Preisach modeling of hysteresis for a pseudoelastic cu-zn-al single crystal. *Journal of applied physics*, **71 (3)**, 1454–1461.

Parvizi, F. and W. Rock, 2003 : The load/deflection characteristics of thermally activated orthodontic archwires. *The European Journal of Orthodontics*, **25 (4)**, 417–421.

Purohit, P. and K. Bhattacharya, 2002 : On beams made of a phase-transforming material. *International journal of solids and structures*, **39 (13)**, 3907–3929.

Qidwai, M. and D. Lagoudas, 2000 : Numerical implementation of a shape memory alloy thermomechanical constitutive model using return mapping algorithms. *Int. J. Numer. Methods Eng*, **47 (6)**, 1123–1168.

Rajagopal, K. R. and A. R. Srinivasa, 1999 : On the thermomechanics of shape memory wires. *Zeitschrift für Angewandte Mathematik und Physik (ZAMP)*, **50 (3)**, 459–496.

Rajagopal, K. R. and A. R. Srinivasa, 2005 : On the bending of shape memory wires. *Mechanics of Advanced Materials and Structures*, **12 (5)**, 319–330.

Raniecki, B., J. Rejzner, and C. Lexcellent, 2001 : Anatomization of hysteresis loops in pure bending of ideal pseudoelastic sma beams. *International journal of mechanical sciences*, **43 (5)**, 1339–1368.

Rao, A. and A. R. Srinivasa, 2013 : Modeling torsion response of shape memory alloy wires and springs by combining thermodynamic principles with preisach models under superelastic conditions. *International Journal of Solids and Structures*, **50 (6)**, 887–898.

Rejzner, J., C. Lexcellent, and B. Raniecki, 2002 : Pseudoelastic behaviour of shape memory alloy beams under pure bending : experiments and modelling. *International journal of mechanical sciences*, **44 (4)**, 665–686.

Sakima, M., M. Dalstra, and B. Melsen, 2006 : How does temperature influence the properties of rectangular nickel–titanium wires ? *The European Journal of Orthodontics*, **28 (3)**, 282–291.

Shaw, J. A. and S. Kyriakides, 1995 : Thermomechanical aspects of niti. *Journal of the Mechanics and Physics of Solids*, **43 (8)**, 1243–1281.

Song, G., N. Ma, and H. Li, 2006 : Applications of shape memory alloys in civil structures. *Engineering Structures*, **28 (9)**, 1266–1274.

Stoeckel, D., 1990 : Shape memory actuators for automotive applications. *Materials & Design*, **11 (6)**, 302–307.

Tonner, R. and N. Waters, 1994 : The characteristics of super-elastic ni-ti wires in three-point bending. part 1 : The effect of temperature. *The European Journal of Orthodontics*, **16 (5)**, 409–419.

Van Humbeeck, J., 1999 : Non-medical applications of shape memory alloys. *Materials Science and Engineering : A*, **273**, 134–148.

Walia, H., W. Brantley, and H. Gerstein, 1988 : An initial investigation of the bending and torsional properties of nitinol root canal files. *Journal of Endodontics*, **14 (7)**, 346–351.

Wayman, C., 1992 : Shape memory and related phenomena. *Progress in Materials Science(UK)*, **36**, 203–224.

Wick, A., O. Vöhringer, and A. Pelton, 1995 : The bending behavior of niti. *Journal de physique. IV*, **5 (8)**, C8–789.

Wilkinson, P., P. Dysart, J. Hood, and G. Herbison, 2002 : Load-deflection characteristics of superelastic nickel-titanium orthodontic wires. *American journal of orthodontics and dentofacial orthopedics*, **121 (5)**, 483–495.